Building Simulation 2003

Eighth International IBPSA Conference
Eindhoven, Netherlands
August 11-14, 2003

REVIEW OF FOUR TURBULENCE MODELS USING TOPOLOGY

Lars Køllgaard Voigt[1], Jens Nørkær Sørensen[1], Jakob Martin Pedersen[1] and Morten Brøns[2]
[1]Department of Mechanical Engineering
Technical University of Denmark
DK-2800 Lyngby, Denmark
[2]Department of Mathematics
Technical University of Denmark
DK-2800 Lyngby, Denmark

ABSTRACT

The validation and development of turbulence models are still important issues related to Computational Fluid Dynamics for ventilation purposes. The present work continues the work initiated by (Voigt, 2002). Four turbulence models are reviewed, the k-ε model, the k-ω model and two blending models combining the k-ε and the k-ω model. The reason for testing the blending models is that the k-ε model is the most robust, while the k-ω model gives a better prediction of the size of the recirculation zone occurring in the Annex 20 room, see (Voigt, 2002). It is found that the blending function responsible for changing from the k-ω model to the k-ε model throughout the boundary layer does not work when simulating the flow in the Annex 20 test case. We analyze the topologies of the numerical flow fields and show that they agree with experiments as precisely as can be expected from a 2D simulation.

INTRODUCTION

The flow in ventilated spaces is complicated since it both consists of regions which are fully turbulent and regions which are purely laminar (Davidson et al, 2000). Thus, accurate predictions of the flow structures is a challenging task using Reynolds Averaged Navier-Stokes (RANS) simulations, since these are generally developed for fully turbulent flow. For calculation of indoor airflows the k-ε model is generally accepted as the best choice. This is because the model is robust and it predicts mean flow variables in acceptable agreement with experiments by (Nielsen,1990). However in some regions the k-ω model gives more accurate results, see (Voigt 2002).
The study showed that the k-ω model predicted the size of the recirculation zone occurring in the Annex 20 room better than the k-ε model. In (Voigt, 2001) 3-D calculations for the flow in the Annex 20 room were carried out. Using the same grid the k-ε model provided a converged solution, while the k-ω did not. Thus, the k-ε model seems to be more numerically robust than the k-ω model. Therefore, we decided to investigate two models combining the k-ε and the k-ω model to test if a combined model possess the numerical robustness of the k-ε model and the accuracy of the k-ω model. The two new models tested were the k-ω baseline model and k-ω shear stress transport model. Both models are developed by (Menter 1994) and it should be underlined that the models were developed for external flows. Since the evaluation of the turbulence models are related to the location and type of critical points a topological approach will be used. The paper is organized as follows: First the test case is presented. Then the topological apparatus is outlined. This is followed by a description of the numerics with special emphasis on the turbulence models. Some experimental results (Pedersen & Meyer, 2002) are analyzed before the numerical results are presented and discussed. Finally we draw our conclusions.

TEST CASE

The test case used for the present study is the 2-D Annex 20 room, see figure 1. The dimensions, excluding the inlet and outlet, were specified in accordance with (Nielsen, 1990). The width of the room is 3 *m* and the flow is isothermal. In the present study, the room is equipped with an inlet and an outlet to avoid numerical problems. The velocity at the inlet is specified in order to obtain *Re*=5000 based on in the inlet height.

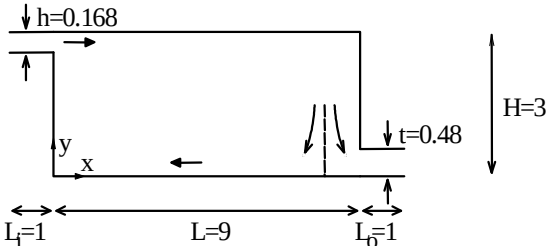

Figure 1: The isothermal Annex 20 room. The inlet and outlet were included in the original test case

TOPOLOGY

Topology in relation to the present study concerns location and classification of critical points in the flow. This knowledge is important since it is the location and type of the critical points which governs the entire flow structure. When we consider 2-D incompressible flows, a critical point in the flow, a so-called in-flow critical point, is characterized by zero velocity, i.e.

$$u = 0 \quad \text{and} \quad v = 0 .$$

On the solid boundaries the velocity is zero by definition. The criterion for having a critical point on a solid boundary, a so-called no-slip critical point, is that

$$\tau_w = 0.$$

For further description see (Hartnack, 1999). Thus, when the flow field is given, it is a straight forward matter to locate the critical points.

It is possible to classify the streamline pattern close to a critical point. For 2-D incompressible flow, the flow field is described by the stream function ψ, taking the definition

$$\dot{x} = \frac{\partial \psi}{\partial y} \quad \text{and} \quad \dot{y} = -\frac{\partial \psi}{\partial x}.$$

Thus, the stream function is a Hamiltonian function for the system**,** see e.g. (Grimshaw, 1990), and there are two non-degenerate possibilities for critical points, a centre or a saddle. Typical streamlines are shown in figure 2.

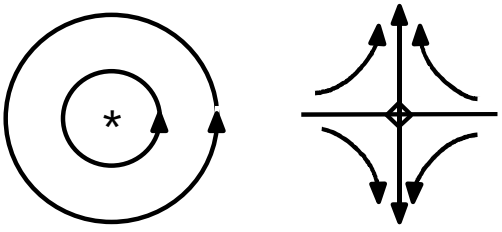

Figure 2: Left: Orbits close to centre, ∗**.** Right: Orbits close to a saddle, ◇**.**

When a no-slip critical point is a saddle point it is relevant to characterize it as either a point of attachment or a point of separation. In figure 3 (left) fluid is approaching a vertical wall and is then ejected downwards below the no-slip critical point and upwards above the no-slip critical point. This point is termed an attachment point. In figure 3 (right) fluid is approaching the no-slip critical point along the wall and is the ejected into the flow domain. This is termed a separation point. More details are given in (Hartnack, 1999).

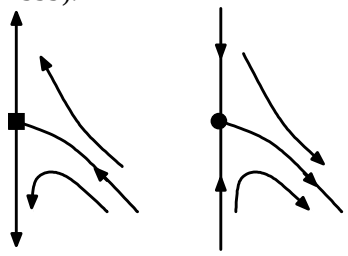

Figure 3: Left: Attachment point, ■, located on a vertical wall. Right: Separation point, ● , located on a vertical wall.

A variety of other critical points can occur in 3-D incompressible flows**.** It is outside the scope of this text to go through these.

However in order to analyze the experimental results we mention the unstable spiral point. This can replace a center if the flow is not exactly 2D. Orbits are shown in figure 4.

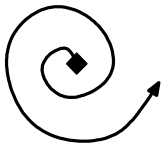

Figure 4: The orbits close to an unstable spiral point, ◆.

NUMERICS

The numerical studies were carried out using the finite volume code EllipSys2D (Michelsen, 1989 & Sørensen, 1995) . The code solves the incompressible, time averaged Navier-Stokes equations. The system of equations are closed using a two-equation turbulence model. Since the present study is focused on turbulence modelling, these are briefly summarized.

The first model tested is the k–ε model (Launder & Sharma, 1974). The transport equations for k and ε are:

$$\frac{\partial k}{\partial t} + u_j \frac{\partial k}{\partial x_j} = \frac{\tau_{ij}}{\rho} \frac{\partial u_i}{\partial x_j} + \frac{\partial}{\partial x_j}\left(\nu + \frac{\nu_t}{\sigma_k} \right) \frac{\partial k}{\partial x_j} - \varepsilon - D$$

$$\frac{\partial \varepsilon}{\partial t} + u_j \frac{\partial \varepsilon}{\partial x_j} = c_{\varepsilon 1} f_1 \frac{\tau_{ij}}{\rho} \frac{\partial u_i}{\partial x_j} \frac{\varepsilon}{k} + \frac{\partial}{\partial x_j}\left(\nu + \frac{\nu_t}{\sigma_k}\right)\frac{\partial \varepsilon}{\partial x_j} - c_{\varepsilon 2} f_2 \frac{\varepsilon^2}{k} + E$$

The second model tested is the k-ω model (Wilcox, 1988)

$$\frac{\partial k}{\partial t} + u_j \frac{\partial k}{\partial x_j} = \frac{\tau_{ij}}{\rho} \frac{\partial u_i}{\partial x_j} + \frac{\partial}{\partial x_j}(\nu + \sigma_{k1}\nu_t)\frac{\partial k}{\partial x_j} - \beta^* \omega k$$

$$\frac{\partial \omega}{\partial t} + u_j \frac{\partial \omega}{\partial x_j} = \frac{\gamma_1}{\nu_t} \frac{\tau_{ij}}{\rho} \frac{\partial u_i}{\partial x_j} + \frac{\partial}{\partial x_j}(\nu + \sigma_{\omega 1}\nu_t)\frac{\partial \omega}{\partial x_j} - \beta_1 \omega^2$$

Compared to the k-ε model no damping functions appear in the k-ω model.

The third model tested is the k-ω baseline (BSL) model (Menter, 1994). This model combines the k-ω model in the inner region of the boundary layer with the k-ε model in the outer region and in the free stream. The transport equations for the turbulent quantities take the form

$$\frac{\partial k}{\partial t} + u_j \frac{\partial k}{\partial x_j} = \frac{\tau_{ij}}{\rho} \frac{\partial u_i}{\partial x_j} + \frac{\partial}{\partial x_j}(\nu + \sigma_k \nu_t)\frac{\partial k}{\partial x_j} - \beta^* \omega k$$

$$\frac{\partial \omega}{\partial t} + u_j \frac{\partial \omega}{\partial x_j} = \frac{\gamma_1}{\nu_t} \frac{\tau_{ij}}{\rho} \frac{\partial u_i}{\partial x_j} + \frac{\partial}{\partial x_j}(\nu + \sigma_\omega \nu_t)\frac{\partial \omega}{\partial x_j} + 2(1 - F_1)\sigma_{\omega 2} \frac{1}{\omega} \frac{\partial k}{\partial x_j} \frac{\partial \omega}{\partial x_j}$$

The blending function is defined by

$$F_1 = \tanh(\arg_1^4)$$

with

$$\arg_1 = \min\left[\max\left(\frac{\sqrt{k}}{0.09\,\omega y}; \frac{500\,\nu}{y^2 \omega}\right); \frac{4\sigma_{\omega 2} k}{CD_{k\omega}\, y^2}\right]$$

where *y* is the distance to the wall and

$$CD_{k\omega} = \max\left(2\sigma_{\omega 2} \frac{1}{\omega} \frac{\partial k}{\partial x_j} \frac{\partial \omega}{\partial x_j}; 10^{-20}\right).$$

When the blending function works properly it should be one near surfaces and zero away from surfaces.

The last model tested is the the k-ω shear stress transport (SST) model (Menter, 1994). This model is similar to the k-ω BSL model, except that the constants for the inner model is slightly changed and the eddy viscosity is now defined as

$$\nu_t = \frac{a_1 k}{\max(a_1 \omega; \Omega F_2)},$$

where Ω is the absolute value of vorticity and

$$F_2 = \tanh(\arg_2^2)$$

where

$$\arg_2 = \max\left(2\frac{\sqrt{k}}{0.09\omega y}; \frac{500\nu}{y^2 \omega}\right)$$

The purpose of the limiter is to account for principal shear stress.

The SIMPLE algoritm was employed for the pressure correction, while the convective terms were discretized to second order using the Second Order Upwind Difference Scheme (SUDS). A convergence criterion of 10^{-5} was used. For the calculation using the k-ε model the solution was converged to machine accuracy. The solution did not change from the solution obtained with a convergence criterion of 10^{-5}.

The governing equations are solved using block structured grids in a cell centered, non-staggered arrangement. The grid was built from blocks of 32x32 cells using 6 blocks in the x-direction and 4 blocks in the y-direction. The inlet and outlet was modelled with one block each. The computational grid is shown in figure 5.

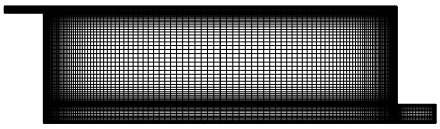

Figure 5: The computational grid

When a calculation has converged the velocities and the value of the stream function is known in every grid point. This information is used for locating critical points. In-flow critical points are found by locating stationary points for the stream function. Points where the stream function has zero partial derivatives will have zero velocity, see (Grimshaw,1990). No-slip critical points on e.g. the floor are found by

monitoring the *u*-component of the velocity in the grid line next to the wall. In points where *u* changes sign we have $\tau_w = 0$ and thus a no-slip critical point exists.

In the following sections we find a separation point on the floor, S_c, and an attachment point on the wall, A_c. For the k-ε model we have determined the location of these points, in order to evaluate if the grid resolution is sufficient. Three different grids were evaluated, a coarse, a medium and a fine build up on blocks of 16x16, 32x32 and 64x64 cells, respectively. Table 1 shows that the *x*-value for the separation point on the floor varies with up to 6 cm for the three grids, while the *y*-value for the attachment point varies about 3 cm. Compared to the differences found between the used turbulence models (see below) the effect from the grid is concluded to be negligible.

	Coarse	Medium	Fine
x value for Sc [*m*]	0.85	0.79	0.84
y value for Ac [*m*]	0.74	0.73	0.76

Table 1: Location of no-slip critical points using different grid resolutions.

EXPERIMENTS

Experimental investigations of the flow in the Annex 20 room have been carried out by (Pedersen & Meyer, 2002). A scale model was constructed, using water as fluid, to facilitate measurements with PIV. The room was scaled with the ratio between the viscosity of air to the viscosity of water. The ensemble averaged velocity vector field in the symmetry plane of the water scale model, taken from (Pedersen & Meyer, 2002), is shown in figure 6. The figure shows the first third of the room length.The sectional stream lines shown in figure 6 were obtained by integrating the particle path along the vector field. It makes sense to consider sectional stream lines in the symmetry plane of the room since the third component of the velocity is zero, i.e. the symmetry plane is invariant.

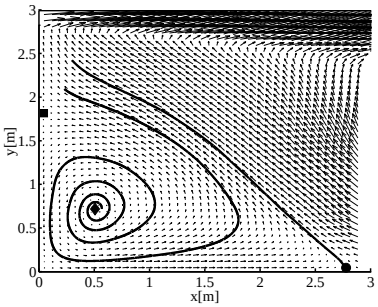

Figure 6: Ensemble averaged velocity vector field in the symmetry plane of the Annex 20 room. Solid lines are sectional stream lines. The figure shows the first third of the room length.

Considering figure 6 we observe a separation point close to the floor at *x*=2.78. Furthermore, an attachment point is observed at the wall at *y*=1.78. Finally an unstable spiral point is observed at (x,y)= (0.51,0.72). Based on these observations, the topology is as sketched in figure 7.

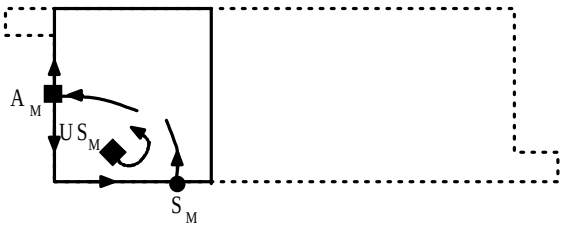

Figure 7: Topology in the symmetry plane of the Annex 20 room. The sketch is based on experiments in a water scale model.

To check the degree of symmetry, the divergence of the mean velocity field has been calculated. Figure 8 shows contours of $-\partial w/\partial z$ calculated from the continuity equation. The maximum values in the region below the wall jet are seen to be of the order of 0.02 s^{-1}. The velocity field is made up of 41*x*42 vectors in total, which gives an interrogation area (IA) size of just below 0.075 *m*. Thus, with a gradient of 0.02 s^{-1} the change in velocity over one IA in the *z*-direction would be 0.0015 m/s. This value is negligible compared to the mean inlet velocity, $u_0 = 0.455$ *m/s*, and hence the flow can be assumed to be symmetric with respect to the centerplane. It is noted that large values of $-\partial w/\partial z$ are found just after the jet inlet. In this region, the tracer particles in a given PIV image were situated outside the measuring domain in the previous image. This general shortcoming of PIV causes a velocity bias towards zero, which explains this unphysical result. However, the error is limited to this region and thus does not affect the results in the lower part of the domain, where the topological analysis is carried out.

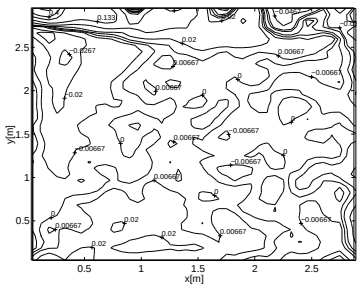

Figure 8: Contours of $-\partial w/\partial z$ calculated from the continuity equation.

RESULTS AND DISCUSSION

The numerical results using the turbulence models outlined above are shown in figure 9-12. Stream lines with constant value of the stream function are used to illustrate the structure of the flow field. Since measurements are available in the lower left part of the room, the critical points occurring in this region of the flow were analyzed by considering the velocity field. In the figures, the types of critical points are inferred by squares, bullets and stars.

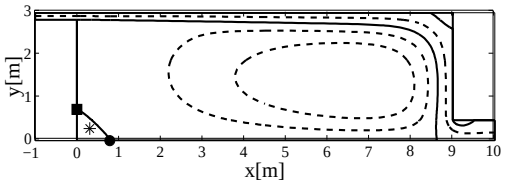

Figure 9: Flow structure for 2-D simulation using the k-ε model. ●:Separation point. ■:Attachment point. ∗:Centre

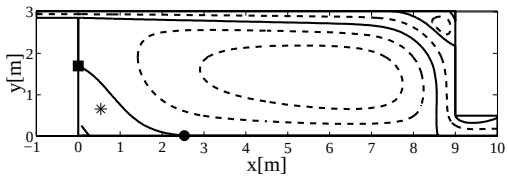

Figure 10: Flow structure for 2-D simulation using the k-ω model. Symbols as in figure 9.

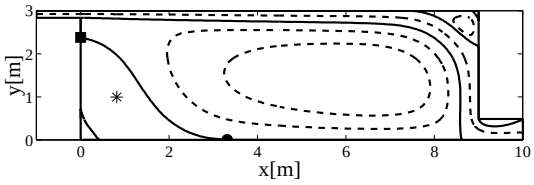

Figure 11: Flow structure for 2-D simulation using the k-ω BSL model. Symbols as in figure 9.

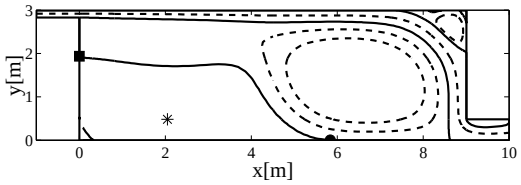

Figure 12: Flow structure for 2-D simulation using the k-ω SST model. Symbols as in figure 9.

From figure 9-12 it is obvious that all turbulence models predict the same topology in the lower left corner of the flow. A separation point is observed at the floor, an attachment point on the wall and the in-flow critical point is a centre. Based on figure 9-12 the numerical topology is sketched in figure 13.

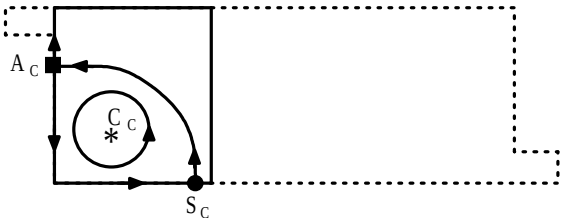

Figure 13: Topology in Annex 20 room. The sketch is based on 2-D simulations.

Comparing figure 13 to the experimental topology in figure 7 shows both similarities and differences. Both simulations and experiments show a separation point on the floor and an attachment point on the wall. However, the simulations suggest that the in-flow critical point is a centre whereas experiments suggest an unstable spiral point. This difference can be explained by the Hamiltonian property of the stream function, which implies that only centres and saddles can be found from a 2-D simulation. Another difference between simulation and experiments is that the separation point and the attachment point are connected by a streamline closing the recirculation zone. In the experiments the no-slip critical points are not connected and the recirculation zone is thus open. This difference is also explained by the Hamiltonian property of the stream function. In the simulations the level of the stream function is chosen so it is zero at the floor and left wall. The stream line emanating from the separation point on the floor must terminate in another critical point with the same value of the stream function. In the present case this stream line terminates in the attachment point on the wall. The conclusion is that the turbulence models give the most accurate topology that can be expected from a 2-D simulation.

The next step is to compare the location of the critical points. Such a comparison was carried out by (Voigt, 2002) who investigated the k-ε model and the k-ω model. The study showed that the k-ω model predicts the location of the critical points within the experimental accuracy, while the k-ε model predicts a recirculation zone that is too small.

The main objective of this study is to test turbulence models blending the k-ε and the k-ω model. It would be expected that such a model should predict a recirculation zone larger than the one found using the k-ε model (figure 9) and smaller than that predicted with the k-ω model (figure 10). However, this was not the

result using the k-ω BSL model (figure 11). Thus, it seems as if the blending function does not work correctly in the present case. The value of the blending function is shown in figure 14. It is obvious that the blending function is not taking the expected value, namely one near surfaces and zero away from surfaces. It should by mentioned that the model was originally developed for predicting the flow about air foils, i.e. for external flows, and thus it seems as if the blending function needs to be redefined for internal flows.

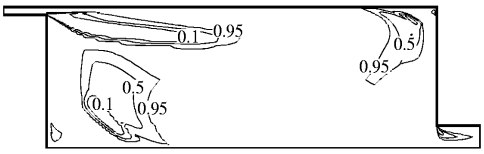

Figure 14: Value of the blending function appearing in the k-ω BSL model. The value should be one near surfaces and zero away from surfaces.

Considering figure 12, the k-ω SST model predicts a recirculation zone larger than that predicted by the k-ω BSL. The difference must be ascribed to the limiter accounting for the principal shear stress. Obviously, the limiter has a strong effect on the size of the recirculation zone. A more detailed study of the limiter is omitted, since the k-ω SST model is a modification of the k-ω BSL model. Thus, it would not be possible to conclude if the effect of the limiter is related to the problems with the k-ω BSL model or the formulation of the limiter.

CONCLUSION

In the present study 2-D simulations of the flow in the Annex 20 room were carried out. Four different turbulence models were tested and the results were compared to PIV experiments from a water scale model of the room. A topological approach was made when comparing the simulations and experiments.

For the PIV experiments, the divergence of the mean velocity field were calculated. The analysis showed that the velocity gradient perpendicular to the centerplane is negligible compared to the mean inlet velocity. Thus, the centerplane can be considered as a symmetryplane. This result is essential for comparing the experiments with 2-D simulations.

Considering the flow structure in the lower left part of the room, the 2-D simulations predicted a separation point on the floor, an attachment point on the wall and an in-flow centre. The separation point and the attachment point were connected by a stream line. The topology was independent of the used turbulence model, but did not agree with the experimental results. The experimental results suggest a separation point on the floor, an attachment point on the wall and an in-flow unstable spiral point. Moreover the separation point and the attachment point was not connected in the experiments. By the topological apparatus it was argued that a 2-D simulation can never capture the experimental topology. The topology obtained by 2-D simulations was concluded to be the best possible considering limitations imposed by the Hamiltonian stream function.

The original k-ω model predicts the location of the critical points well, while the k-ε model under predicts the size of the recirculation zone. The k-ω baseline model blends the k-ε model away from walls with the k-ω model near walls. However, the model predicted a recirculation zone larger than that predicted by the k-ω model. The blending function was investigated and it turned out that the blending function does work as intended for this flow. Finally, the k-ω shear stress transport model predicts the largest recirculation of the used models. The effect of the limiter was not investigated further, since the k-ω shear stress transport model is a modification of the k-ω baseline model.

ACKNOWLEDGEMENT

The author's would like to thank Dan N. Sørensen who developed the grid generator used in this work. Furthermore, we thank the International Centre for Indoor Environment and Energy (ICIEE) and Myhrwolds Fond, who financed this work. Finally, we thank the High Performance Computing Centre at DTU who provided computer resources.

REFERENCES

Davidson, L., Nielsen, P.V. & Topp, C. (2000), "Low-Reynolds Number Effects in Ventilated Rooms: a Numerical Study", ROOMVENT 2000, vol. 1, 307-312.

Grimshaw, D., (1990), "Nonlinear Ordinary Differential Equations", Blackwell Scientific Publications", 276-314.

Nielsen, P.V., (1990), "Specification of a Two-dimensional Testcase, IEA Annex 20 Research Item 1.45", Technical Report, University of AAlborg, Denmark.

Hartnack, J.N., (1999), "Streamline Topologies near a Fixed Wall using Normal Forms", Acta Mechanica, vol. 136, issue 1, 55-75.

Launder, B.E. & Sharma, B.I. (1974), "Application of the Energy Dissipation Model of Turbulence to the Calculation of Flow near a Spinning Disk", Letters in Heat and Mass Transfer, vol. 1, No. 2.

Menter, F.R. (1994), "Two-equation Eddy-Viscosity Turbulence Models for Engineering Applications", AIAA Journal, Vol. 32, No. 8, August, 1598-1605.

Michelsen, J.A., (1989), "Solution of the Navier-Stokes equations on general Non-orthogonal Meshes", AFM 89-08, Department of Fluid Mechanics, DTU.

Pedersen, J.M. & Meyer, K.E., (2002), "POD Analysis of Flow Structures in a Scale Model of a Ventilated Room", Experiments in Fluids 33, 940-949.

Sørensen, N.N., (1995), "General Purpose Flow Solver Applied to Flow over Hills", Ph.D. Thesis, Risø National Laboratory, Denmark, Risø-R-827(EN) .

Voigt, L.K., (2001), "Navier-Stokes Simulation of Airflow in Rooms and Around a Human Body", Ph.D. Thesis, Department of Mechanical Engineering, Fluid Mechanics Section, DTU.

Voigt, L.K., (2002), "Validation of Turbulence Models using Topological Aspects", ROOMVENT 2002, 173-176

Wilcox, D.C., (1988), "Reassesment of the Scale-Determining Equation for Advanced Turbulence Models", AIAA Journal, Vol. 26, No. 11, November, 1299-1310.

NOMENCLATURE

LATIN

a_1: Constant in the limiter in the k-ω SST model
A_c: Computational determined attachment point
$c_{\varepsilon 1}$,$c_{\varepsilon 2}$: Empirical constants in the Launder & Sharma model
D: Correction term in the Launder & Sharma model
E: Correction term in the Launder & Sharma model
f_1,f_2: Damping functions
F_1: Blending function
F_2: Limiter
h: Height of inlet
k: Turbulent kinetic energy
L: Length of room
L_i: Length of inlet
L_o: Length of outlet
S_c: Computational determined separation point
t: Height of outlet
u: Horizontal component of velocity
v: Vertical component of velocity

GREEK

β_1, β^*: Constant in the k-ω model
ε: Dissipation of turbulent kinetic energy
γ_1: Constant in the k-ω model
ω: Specific dissipation rate
τ_{ij}: Stress tensor
τ_w: Wall shear stress
ν: Kinematic viscosity
ν_t: Eddy viscosity
σ_k: Turbulent Prandtl number
σ_ε: Turbulent Prandtl number
σ_{k1}: Turbulent Prandtl number
$\sigma_{\omega 1}$, $\sigma_{\omega 1}$: Turbulent Prandtl number
Ω: Absolute value of vorticity